

Deformation Microstructure Under Nanoindentations in Cu Using 3D X-Ray Structural Microscopy

Wenge Yang¹, B.C. Larson¹, G.M. Pharr^{1,2}, G.E. Ice¹, J.G. Swadener³, J.D. Budai¹, J.Z. Tischler¹, and Wenjun Liu¹

¹Oak Ridge National Laboratory, Oak Ridge, Tennessee 37831

²University of Tennessee, Knoxville, Tennessee 37996

³MST-8, Los Alamos National Laboratory, Los Alamos, NM 87545, USA

ABSTRACT

We have used a recently developed x-ray structural microscopy technique to make nondestructive, submicron-resolution measurements of the deformation microstructure below a 100mN maximum load Berkovich nanoindent in single crystal Cu. Direct observations of plastic deformation under the indent were obtained using a ~0.5 μm polychromatic microbeam and diffracted beam depth profiling to make micron-resolution spatially-resolved x-ray Laue diffraction measurements. The local lattice rotations underneath the nanoindent were found to be heterogeneous in nature as revealed by geometrically necessary dislocation (GND) densities determined for positions along lines beneath a flat indent face and under the sharp Berkovich indent blade edges. Measurements of the local rotation-axes and misorientation-angles along these lines are discussed in terms of crystallographic slip systems.

INTRODUCTION

Fundamental aspects of materials properties and evolution are being investigated in increasing detail both experimentally and computationally [1-3]; accordingly, the importance of detailed microstructural information on the plastic deformation of materials on mesoscopic length scales (tenths to hundreds of microns) is increasing as well [4]. As mechanical devices decrease in size, a large effort has been directed toward understanding local microstructural distributions and evolution. This is especially true with respect to dislocation structures, where it is important to understand the fundamental processes and micro-mechanisms associated with plastic deformation. In most circumstances, plastic deformation is controlled by dislocation motion and self-arrangement [3,4]. Nanoindentation experiments have long been a very useful method for materials characterization as an overall experimental tool for evaluating basic properties of materials from small samples [5,6]. Nanoindentation is known to produce a range of plastic deformation structures under indent tips on mesoscopic length scales and analyses often result in size- and depth-dependent hardness effects [7-9]. Atomic force microscopy (AFM), transmission electron microscopy (TEM), and finite element methods (FEM) have been used to investigate the hardness, indentation loading curves, phase transitions, and dislocation structure [7,10,11]. However, these experimental tools provide detailed microstructure information only from surface layers, thin sections, or thin film structures. Until recently, nondestructive 3D microstructural probes with the submicron, intra-granular spatial resolution required to investigate the heterogeneous deformation induced below nanoindents have not been available.

High brilliance synchrotron x-ray sources and high precision, achromatic, x-ray focusing optics now make it possible to focus polychromatic, hard x-ray beams to submicron sizes

[12,13]. This capability is complementary to earlier $>10\ \mu\text{m}$ resolution x-ray microbeam developments [14,15]. The most prominent advantages of hard x-rays are penetration depths from tens to hundreds of microns (or greater) and the ability to make high angular precision orientation determinations. By combining submicron diameter incident x-ray beams with the differential-aperture x-ray microscopy (DAXM) depth profiling technique [12] at the Advanced Photon Source, it is now possible to obtain local orientation and residual stress from submicron voxels (volume elements) of materials. Here we report micron resolution nondestructive DAXM measurements of local lattice curvatures under a 100 mN Berkovich indent, and we discuss possible dislocation slip systems consistent with the deformation microstructure.

EXPERIMENT

Figure 1 displays the experimental microbeam diffraction geometry used on the MHATT-CAT and UNI-CAT beamlines at the Advanced Photon Source, Argonne National Laboratory [13]. A polychromatic (i.e. white) synchrotron x-ray beam is focused by elliptically figured K-B mirrors to $\sim 0.5\ \mu\text{m}$ diameter before it hits the sample and a CCD area detector is used to collect the Laue diffraction images. A $50\ \mu\text{m}$ diameter Pt wire is used as a knife-edge absorption profiler to probe the spatial distribution of Bragg diffracted intensity from the sample as described previously [12]. By taking submicron steps of the Pt wire along the sample surface and subtracting CCD images taken before and after each step, one can obtain the differential intensity distribution that passes through the pinhole-like camera (the submicron gap between the two wire positions). Computer reassembling of the differential intensity distribution for each wire step makes it possible to collate and reconstruct full Laue diffraction images from submicron voxels along the penetration direction. By automatic indexing and crystallographic orientation analysis, the resulting depth resolved Laue diffraction patterns, spatially resolved measurements of the deformation structure along the microbeam are obtained. Since complete white-beam diffraction patterns are generated by each segment of material irradiated by the x-ray microbeam, continuous rotations inside a grain or a single crystal can be resolved spatially; this point-to-point intra-granular measurement capability distinguishes the DAXM technique from other existing 3D x-ray microscopy techniques [14,15] that have been developed and applied to grain-boundary mapping and investigation of grain-average polycrystalline deformation modes.

A dislocation free Cu single crystal with a $\langle 111 \rangle$ plane normal was subjected to a 100 mN maximum load indent using a Berkovich tip. The three indent edges of the Berkovich indent were lined up within about 8 degrees of the three $\langle 110 \rangle$ type directions in the surface plane of sample as shown in Figure 2. The AFM measurement shows that there is no pile-up at the edges of the indentations for this soft copper sample. For performing the x-ray microbeam measurements, the surface of the sample was oriented at an angle of 45° with respect to the incident beam so that the microbeam could penetrate $\sim 30\ \mu\text{m}$ below the surface, limited ultimately by beam attenuation as shown in Figure 1.

Both the $\langle 111 \rangle$ oriented sample and the triangular pyramid shape of the Berkovich indenter have three fold symmetry, thus the diffraction patterns can be expected to have mirror symmetry with respect to the center plane of the indent (within the ~ 8 degree rotation of the indent to the $\langle 110 \rangle$ orientation, of course). Although DAXM measurements have been made over full slices through the indent, in this short report two positions have been chosen for discussion; they are indicated by positions A and B in Figure 2. At position A, the x-ray microbeam enters the sample in the middle of a flat blade face and penetrates the sample for $\sim 30\ \mu\text{m}$ underneath this

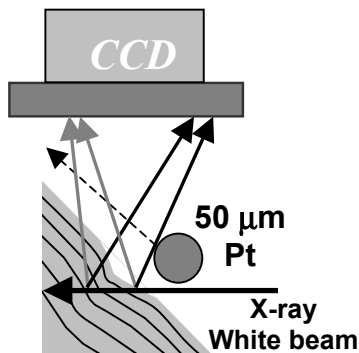


Figure 1. Schematic of the 3D x-ray microscope sample, beam, and profiler.

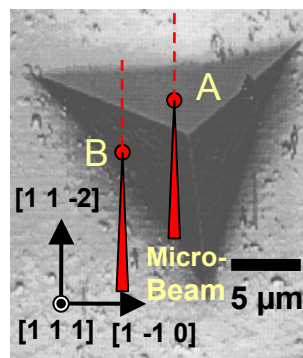


Figure 2. AFM image of 100 mN Berkovich indent in Cu. A and B indicate the microbeam entry points and the dashed lines show the penetration direction.

flat face; the diffracted intensity diffracts upward into the detector for all positions along the penetration depth.

At position B, the microbeam initially penetrates the area underneath the left blade of the indent and then penetrates under the upper blade, after traveling through the region under the sharp blade edge where the upper and left indenter blades meet. Therefore, for position A, only one indent blade has an effect on the local deformation microstructure, while for position B, a combination of effects from the left and the upper indenter blades is present as well as from their sharp intersection.

RESULTS

Figure 3 displays both depth integrated and depth resolved results from position A. Figure 3(b) is the depth integrated (i.e. full) Laue pattern over the whole penetration distance. To large extent, the lattice is rotated about an axis parallel to the horizontal $[1-10]$ axis in the sample surface plane; this is clear even without detailed analysis because each (hkl) diffraction spot in the Laue pattern is found to elongate in only the vertical direction. Figure 3(a) displays an enlarged picture of the (hhh) peak. Since white Laue patterns represent a one-to-one mapping of local plane orientations onto the CCD area detector, the uneven (lumpy) intensity distribution of the streak indicates qualitatively a heterogeneous distribution of lattice rotations as a function of depth along the microbeam. A quantitative depth resolved (111) pole figure (obtained by the DAXM analysis) is displayed in Figure 3(c).

The enlarged (111) pole figure shows the DAXM determined orientation for successive micron positions as a function of depth along the microbeam. The “x” marks in Figs. 3(a) and 3(c) indicate the undeformed orientation as a reference. The local misorientation angle (i.e. local orientation compared to the orientation of the following μm) as a function of depth is plotted in Figure 3(d). For position A, the rotation axis was found to lie approximately along the $[1 -1 0]$ direction, corresponding to the direction of the edge of the indentation of the upper blade.

Similar measurements and analyses performed at position B are displayed in Figure 4. Both the Laue images and the detailed depth-resolved pole figure analyses reveal a more complicated microstructural deformation, as might be expected for a beam traversing below two different indent faces as well as under the sharp blade-edge region between the two faces. The triangle shaped form of the (111) pole figure indicates immediately that, unlike the case for position A, the local rotation axes change discontinuously with depth along the beam penetration direction.

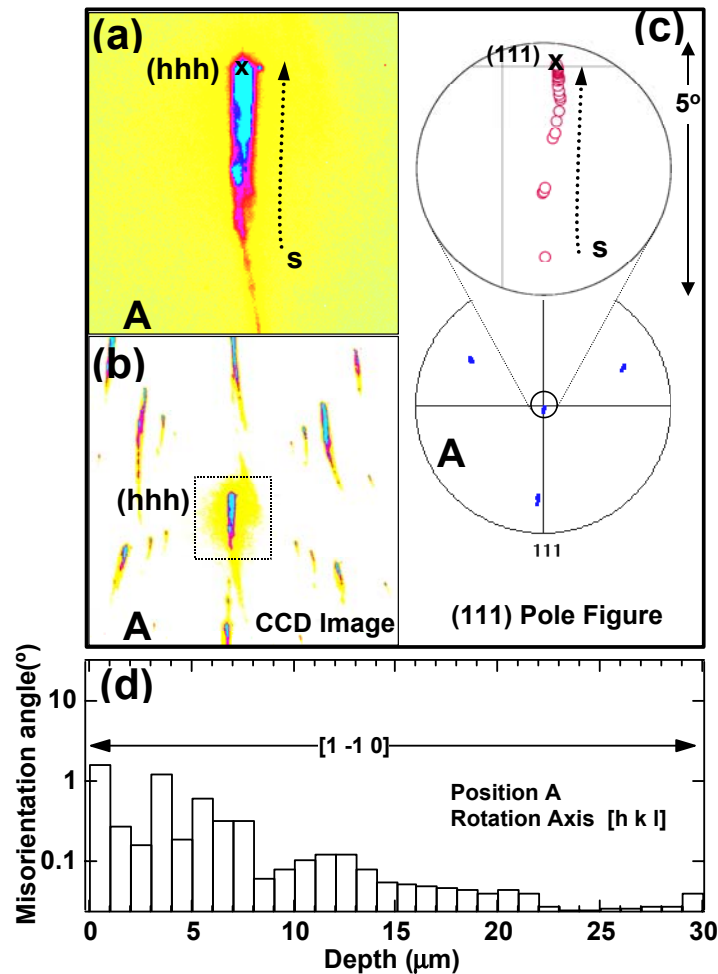


Figure 3. Enlarged (hhh) Laue pattern (a) and full Laue pattern (b) at sample position A. (c) depth resolved (111) pole figure; (d) log plot of local misorientation angles at position A as a function of penetration depth with nominal rotation axis $[1 -1 0]$ indicated.

This is shown quantitatively in Figure 4(d), where both the magnitude of the micron-by-micron misorientations and the rotation axes are indicated.

We note that initially (i.e. near the surface at position B) the rotation axis is approximately the $[1 0 -1]$; this is consistent with rotations immediately under the flat faces being along one of the $\langle 110 \rangle$ type directions defined by the edges of blade faces. However, as the beam penetrates under the sharp blade edge a few microns further, there is a large, abrupt rotation around the $[3 2 -3]$ direction. This abrupt change in direction is followed rotations direction around the $[1 -2 0]$ axis. These $[1 0 -1]$, $[3 2 -3]$ and $[1 -2 0]$ rotation axes correspond to the three dotted arrows in the expanded pole figure in Figure 3; the deepest material has a $[1 -1 0]$ rotation axis as in A.

DISCUSSION

In face centered cubic (fcc) structure materials, the primary dislocation systems have Burgers vector $\langle 1 1 0 \rangle / 2$, line directions along $\langle 1 1 2 \rangle$ (edge type) or $\langle 1 1 0 \rangle$ (screw type) and $\{1 1 1\}$ slip planes. Since none of the rotation axes involved in positions A or B are along a $\langle 1 1 2 \rangle$ type

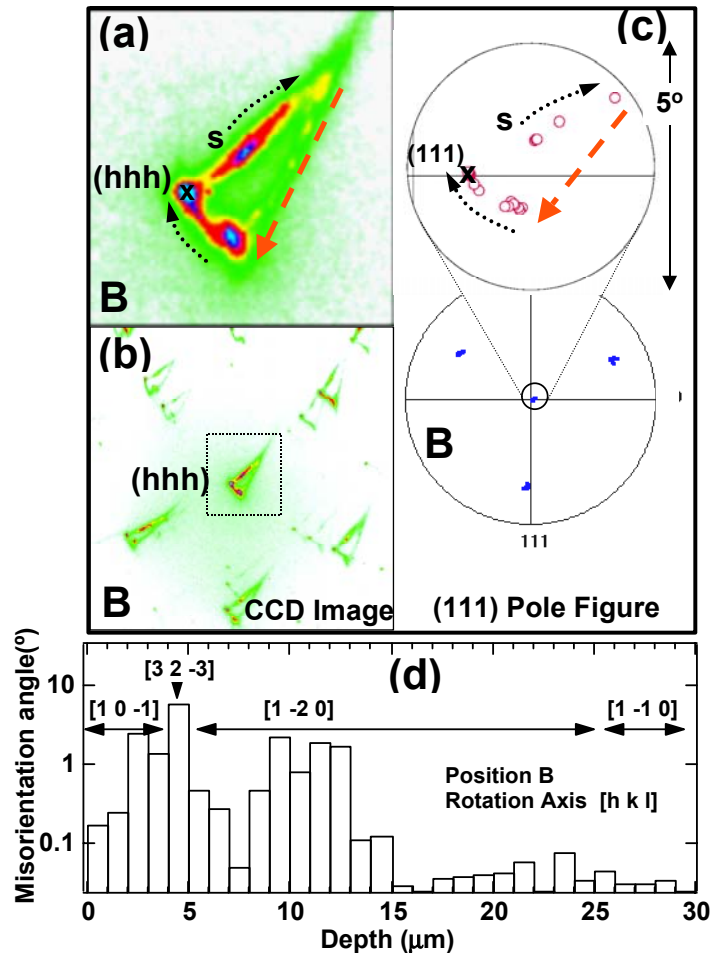


Figure 4. Enlarged (hhh) Laue pattern (a) and full Laue pattern (b) at sample position B. (c) depth resolved (111) pole figure; (d) log plot of local misorientation angles at position B as a function of penetration depth with nominal rotation axes indicated.

direction, there must be at least two slip systems active simultaneously in all cases to account for the necessary local lattice curvature measurements. A simulation of Laue patterns with multiple slip systems has been reported elsewhere [16]. Since the density of GNDs is linear in the misorientation angle [3], we can estimate the local GND density along the x-ray beam direction. Of course, the lattice curvature obtained by comparing neighboring orientations along a single direction is a measure of the GND density in this direction only, and thus represents a lower limit for the full dislocation density. Although full 3D GND measurements are in progress, it is likely that the linear GND densities are within a factor of ~ 2 of the 3D result here.

Following the formulas for GND density proposed by Needleman [3], we find the GND density to range up to $\sim 2 \times 10^{10}/\text{cm}^2$ and $\sim 7 \times 10^{10}/\text{cm}^2$ at measurement points A and B, respectively. The presence of the sharp changes in orientation is the signature of dislocation wall patterning under the indent. Dislocation patterning is to be expected for deformation in an fcc metal like Cu [1], and indeed dislocation structures have been reported using TEM near surfaces in a number of nanoindented materials [11, 17]. However, the results presented here represent the first quantitative, nondestructive observations of dislocation structures with micron spatial resolution for mesoscopic length scales deep under nanoindented surfaces. Finite element method (FEM) simulations and strain gradient plasticity predict the influence of indenter size

and depth on hardness reasonable well for certain length scales [2,7] using simple dislocation loop models. However, the dense distributions of forest dislocations predicted by FEM to be localized below indents are in contrast to the sharp (slip band) rotations observed here. Slip bands would reduce dislocation densities immediately under indents by channeling dislocations far away from the indent tip region. This would reduce the hardness of the deformed material beneath indents and impact nanoindentation hardness measurements. Therefore, detailed information on the three-dimensional dislocation microstructure as a function of indenter depth is critical for modeling indentation hardness measurements and for understanding the fundamental aspects of plastic deformation in general. 3D x-ray microscopy measurements of the microstructure below indents in Cu are in progress over the entire indent volume.

CONCLUSIONS

We have performed nondestructive, submicron-resolution 3D measurements of deformation microstructure in nanoindented Cu. Spatially resolved measurements of local orientations and (linear) geometrically necessary dislocation (GND) densities have been obtained using the DAXM x-ray structural microscopy technique. Berkovich indents are observed to generate strong dislocation patterning in copper.

ACKNOWLEDGMENTS

Research sponsored by the Department of Energy, Office of Science, Division of Materials Sciences at ORNL managed by UT-Battelle, LLC, under contract DE-AC05-00OR2272. Work was performed on the MHATT-CAT and UNI-CAT beamlines at the APS; the operation of the APS is sponsored by the DOE.

REFERENCES

- [1] D.A. Hughes and N. Hansen, *Acta Mater.*, **45**, 3871 (1997).
- [2] Y. Huang, Z. Xue, H.Gao, W. Nix and Z.C. Xia, *J. Mater. Res.*, **15**, 1786 (2000).
- [3] A. Needleman, *Acta Mater.*, **48**, 105 (2000).
- [4] D.A. Hughes, D.C. Chrzan, Q. Liu and N. Hansen, *Phys. Rev. Lett.*, **81**, 4664, (1998).
- [5] J.B. Thompson *et al.*, *Nature*, **414**, 773 (2001).
- [6] B.R. Lawn, N.P. Padture, H.D. Cai and F. Guiberteau, *Science*, **263**, 1114 (1994).
- [7] Z. Xue, Y. Huang, K.C. Hwang and M. Li, *J. Eng. Mater. Tech.*, **124**, 371 (2002).
- [8] Q. Ma and D.R. Clarke, *J. Mater. Res.*, **10**, 853 (1995).
- [9] J.G. Swadener, E.P. George, G.M. Pharr, *J. Mech Phys. Solids*, **50**, 681 (2002).
- [10] S. Harvey, H. Huang, S. Venkataraman and W.W. Gerberich, *J. Mater. Res.*, **8**, 1291 (1993).
- [11] J.E. Bradby *et al.*, *Appl. Phys. Lett.*, **77**, 3749 (2000).
- [12] B.C. Larson, W. Yang, G.E. Ice, J.D. Budai and J.Z. Tischler, *Nature*, **415**, 887 (2002).
- [13] G.E. Ice and B.C. Larson, *Adv. Eng. Mat.*, **2**, 643 (2000).
- [14] H.F. Poulsen *et al.*, *J. Appl. Cryst.*, **34**, 751 (2001).
- [15] L. Margulies, G. Winther, and H.F. Poulsen, *Science*, **292**, 2392 (2001).
- [16] R. Barabash, G.E. Ice, B.C. Larson, G.M. Pharr, K.-S. Chung, and W. Yang, *Appl. Phys. Lett.*, **79**, 4 (2001).
- [17] Y.L. Chiu and A.H.W. Ngan, *Acta Mater.*, **50**, 2677 (2002).